Dynamical Behavior Near a Liquid−Liquid Phase Transition in Simulations of Supercooled Water

Peter H. Poole,*[,†] Stephen R. Becker,[‡,§] Francesco Sciortino,*[,¶] and Francis W. Starr*[,‡]

[†]Department of Physics, St. Francis Xavier University, Antigonish, Nova Scotia B2G 2W5, Canada,

[‡]Department of Physics, Wesleyan University, Middletown, Connecticut 06459, United States

[¶]Dipartimento di Fisica and CNR-ISC, Università di Roma La Sapienza, Piazzale Aldo Moro 2, I-00185 Rome, Italy

ABSTRACT: We examine the behavior of the diffusion coefficient of the ST2 model of water over a broad region of the phase diagram via molecular dynamics simulations. The ST2 model has an accessible liquid−liquid transition between low-density and high-density phases, making the model an ideal candidate to explore the impacts of the liquid−liquid transition on dynamics. We locate characteristic dynamical loci in the phase diagram and compare them with the previously investigated thermodynamic loci. The low-density liquid phase shows a crossover from non-Arrhenius to Arrhenius behavior, signaling the onset of a crossover from fragile-to-strong behavior. We explain this crossover in terms of the asymptotic approach of the low-density liquid to a random tetrahedral network and show that the temperature dependence of the diffusion coefficient over a wide temperature range can be simply related to the concentration of defects in the network. Our findings thus confirm that the low-density phase of ST2 water is a well-defined metastable liquid.
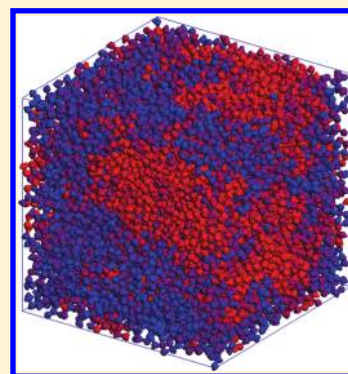
INTRODUCTION

It has long been appreciated that water, the most important of all liquids, defies description in terms of simple liquid behavior in most respects.[1,2] Many of the anomalies of the thermodynamic and transport properties can be attributed to the hydrogen bonds that dominate the intermolecular interactions.[3−8] Of the many important studies of water conducted over the last several decades, the 1992 proposal that a liquid−liquid phase transition (LLPT) occurs in supercooled water has had a particularly significant impact on water research.[9] In this proposal, two phases of liquid water, a low density liquid (LDL) and a high density liquid (HDL), become distinct below a critical point located in the supercooled regime of the phase diagram. Stanley and co-workers have pursued the implications of this proposal over the last 20 years,[9−38] and much has been learned about the impact of a liquid−liquid transition on the properties of water and related systems.[39,40]

The LLPT proposal remains controversial because its confirmation via experiments on the bulk liquid has been thwarted by rapid ice nucleation at the conditions at which the critical point is predicted to occur; bulk studies of the ice melting lines provide indirect evidence of a transition.[18] The central strength of the LLPT proposal is that it rationalizes the thermodynamical and dynamical anomalies of the supercooled liquid while, at the same time, it accounts for the occurrence in experiments of two widely different forms of amorphous solid water (low density and high density amorphous ice) as the subglass-transition manifestations of the LDL and HDL phases.[12,27,29,41−44] Indeed, the possibility of a LLPT has now been investigated across the entire class of liquids in which tetrahedral bonding dominates the local structure. This class of systems includes water, Si,[45] SiO_2,[46] and BeF_2,[47] as well as nanoparticle liquids tailored to exhibit

tetrahedral interactions.[48,49] Additionally, it has also been shown that liquids with symmetric interactions, but with a competition between low density and high density packings, may also exhibit LLPT behavior.[22,26,28,50]

Due to the challenges imposed by crystallization on experiments of supercooled water, computer simulations have played a central role in the development of the LLPT proposal for water, and other tetrahedral liquids. Although a LLPT occurs in a variety of water models, one of the most accessible and clearest examples is in the venerable ST2 model,[51] one of the earliest point-charge models for water. "ST2 water" has been extensively studied to clarify the nature of such a LLPT, in particular with regard to thermodynamic and structural properties.[9,11,15,16,52−55] Though much is known about the dynamics of ST2 water,[6,34,52,56−60] a comprehensive study of the dynamical properties comparable in scope to the thermodynamic studies is lacking. Therefore, in the present work, we focus on the dynamical properties of the ST2 model over a wide range of states that encompasses the vicinity of the LLPT. We show that there are striking differences in the nature of the dynamics of the HDL and LDL phases. The LDL phase presents a particular challenge, as the relaxation time of the liquid increases extremely rapidly with decreasing temperature T. However, our results demonstrate that the equilibrium dynamical properties of the LDL phase can be understood from the behavior observed in the region accessible to our simulations. These results emphasize the central role
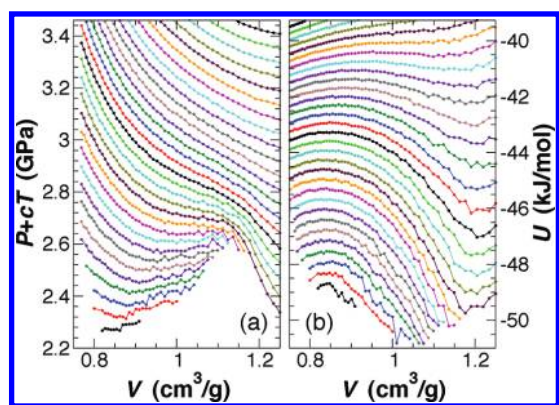
Figure 1. (a) Pressure P and (b) potential energy U as a function of volume V along isotherms for ST2 water, from our $N = 1728$ simulations. In both panels, we show isotherms from $T = 200$ to 350 K, in 5 K steps, from bottom to top. In (a), each isotherm is shifted by cT, with $c = 10$ MPa/K, to facilitate comparison of the curves. In (b), the minima of U occurring at low T and in the vicinity of $V = 1.2$ cm^3/g ($\rho = 0.83$ g/cm^3) identify conditions at which a particularly well developed random tetrahedral network occurs in the liquid.

of the developing network of hydrogen bonds for understanding the behavior of the liquid, especially of the LDL phase.

SIMULATIONS

Our data are generated via molecular dynamics simulations of the ST2 potential.[51] The simulations follow the same protocol as those in ref 53. Specifically, we attempt simulations at thermodynamic state points in the density range $\rho = 0.80-1.20$ g/cm^3 at intervals $\Delta\rho = 0.01$ g/cm^3, and the temperature range $T = 200-400$ K at intervals of $\Delta T = 5$ K. At each state point considered, we simulate $N = 1728$ molecules, unless noted otherwise. We are able to equilibrate the liquid at all chosen densities for $T \geq 255$ K; for $T < 255$ K, the lowest density studied is limited by the extreme length of simulation required. In total, we examine more than 1500 different state points. The configurations used to start simulations are the final configurations from ref 53, where a detailed equation of state (EOS) of ST2 water was evaluated. Each simulation is run until the mean-squared displacement (MSD) of oxygen atoms reaches 1 nm^2 (roughly three interparticle spacings), much longer than needed to observe diffusive behavior. We use an integration time step of 1 fs and employ the Berendsen heat bath with a time constant of 2 ps to control T during the production run, to compensate for a possible minor drift of the energy in the very long simulation runs. Periodic boundaries are used to minimize size effects. The electrostatic potential is truncated at 7.8 Å, and the energy and pressure are corrected using the reaction field method.[61] Careful treatment of long-ranged forces using the Ewald method shows the same qualitative behavior (including the liquid—liquid transition), but the quantitative location of the critical point and transition line differs by a small amount.[54] Trajectory information was written to disk every 100 fs for $T \geq 250$ K, and every 10 ps for $T < 250$ K.

Figure 1 summarizes the thermodynamic properties of the ST2 liquid in the region examined here. Figure 1a shows the pressure P as a function of volume V along isotherms. As T decreases, these isotherms first inflect and then become progressively flatter, leading to the realization of a liquid—liquid critical point at which $(\partial P/\partial V)_T = (\partial^2 P/\partial V^2)_T = 0$. The critical point conditions in ST2 water have been estimated to occur at $T_c = 247 \pm 3$ K, $P_c = 185 \pm 15$ MPa, and $\rho_c = 0.955 \pm 0.01$ g/cm^3.[54,55]

Figure 1b presents the variation of the potential energy U as a function of V along isotherms of the liquid. As noted in previous work,[16,21,62] the emergence with decreasing T of significant negative curvature in the energy along isotherms is a thermodynamic signature of the approaching liquid—liquid instability. Specifically, to be stable with respect to phase separation, the Helmholtz free energy A must have positive curvature $(\partial^2 A/\partial V^2)_T > 0$. Because $A = U - TS$ (where S is entropy), the negative curvature shown in Figure 1b indicates an energetic driving force for phase separation. This energetic signature appears well above T_c, and thus provides a useful indicator, suggesting the likely phase separation at lower T, because the contribution from TS to the free energy becomes progressively smaller on cooling.[16,21] It is also interesting to observe the minima of U occurring at low T and in the vicinity of $V = 1.2$ cm^3/g ($\rho = 0.83$ g/cm^3). The presence of this minimum has also been observed in several other models of tetrahedral liquids,[16,62−64] and signals the optimal network volume (or density), i.e., the conditions at which a particularly well developed random tetrahedral network occurs in the liquid. Indeed, hydrogen bonding requires a well-defined distance and orientation to be effective, and at the optimal density (which is usually close to the fully bonded open crystal density) geometric constraints allow the establishment of a fully bonded disordered network.

DIFFUSIVITY OF THE ST2 MODEL

For each state point simulated, we calculate the mean-squared displacement $\langle r^2(t) \rangle$ and evaluate the diffusion coefficient from the Einstein relation

$$D = \lim_{t \to \infty} \frac{\langle r^2(t) \rangle}{6t} \tag{1}$$

Here $\langle ... \rangle$ represents an average over all molecules and time origins. Because we have more than 1500 state points to consider, we automate the evaluation of D by a linear fit of $\langle r^2(t) \rangle$ for all data such that $\langle r^2(t) \rangle > 0.5$ nm^2, a restriction that ensures that all fitted data are well within the diffusive regime.

We first consider D along isotherms, as shown in Figure 2. For $T < 335$ K, D exhibits a (weak) maximum with increasing ρ or P, as known experimentally.[65,66] This feature is normally attributed to the breaking of hydrogen bonds with increasing density, which allows for increased diffusion, until packing considerations become dominant and D decreases. As compared with water, the ST2 model overestimates the pressure of the maximum in D, which is not surprising given that ST2 overemphasizes the tetrahedral structure relative to water.[67] Hence, there exists a locus of points (which we denote D_{max}) on the EOS surface at which D is a maximum along isotherms; the shape of this locus in the phase diagram is discussed below. Figure 2 also includes data obtained for $T < T_c$. The filled data points indicate simulations in the unstable regime where our system (simulated at constant volume) is phase separated into regions of LDL and HDL. The values of D in this region thus reflect a weighted average over the LDL and HDL phases. We note that D decreases by nearly 2 orders of magnitude as the system progressively transforms from pure HDL to pure LDL along the lowest T isotherms.

We next present the T-dependence of D along isochores and isobars in Figure 3. At high T, D is described by the expected
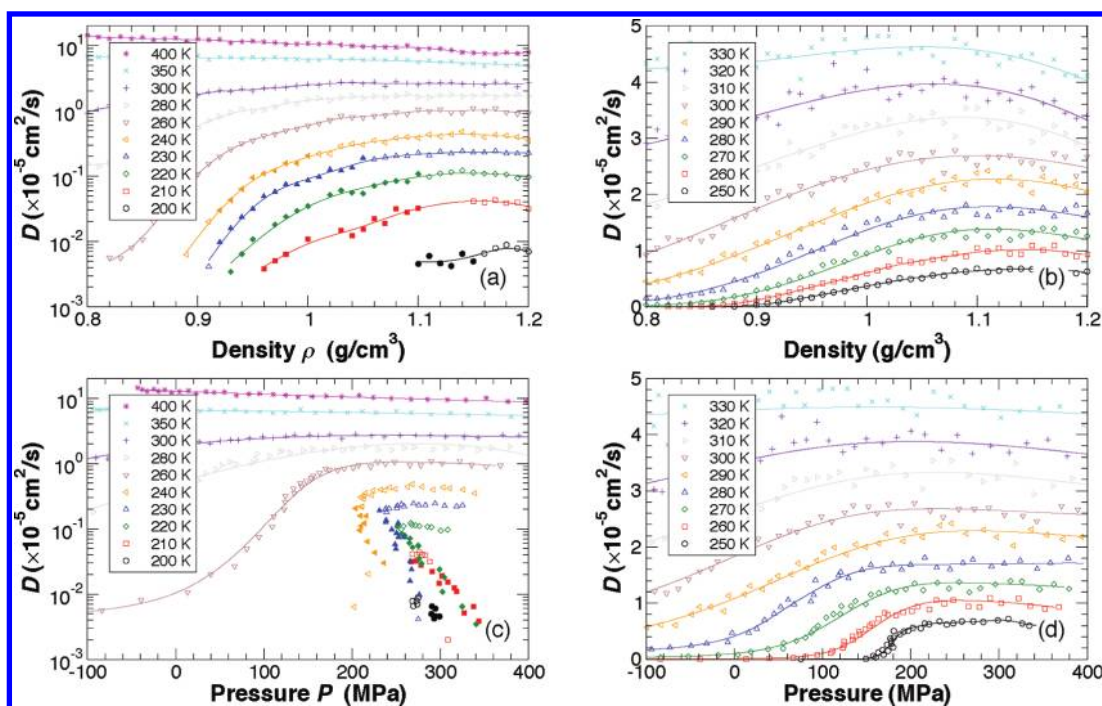
Figure 2. Diffusion coefficient D along isotherms as a function of density ρ ((a) and (b)) or pressure P ((c) and (d)). The lines are intended only as a guide for the eye. We plot only a selection of our available isotherms to avoid overcrowding in the figure. We show both log ((a) and (c)) and linear ((b) and (d)) scales to cover a broad range of D (log scale) and to show the form of the maxima of D (linear scale). The solid symbols indicate state points in the unstable zone of the liquid−liquid coexistence region. Note that D is a multivalued function of P along isotherms for $T < 250$ K because P is a nonmonotonic function of ρ in the coexistence region along these isotherms.

Arrhenius behavior

$$D = D_0 \exp[-E/k_B T] \qquad (2)$$

where E is the activation energy for diffusion and D_0 is the limiting high-T diffusion coefficient (both determined from fitting eq 2 to the data). On cooling below a temperature T_A, D exhibits so-called "super-Arrhenius" behavior, where D decreases faster than expected relative to the high-T behavior. This rapid decrease is typical of glass-forming liquids as they approach the glass transition temperature T_g. We estimate T_A for D along either isochores or isobars by finding that T at which $k_B T/E$ $\ln(D/D_0) > 1.02$; by construction, this quantity must equal unity for high-T Arrhenius behavior.[68]

The non-Arrhenius behavior of D for many glass-forming liquids is well-accounted for by the mode-coupling theory (MCT) for the glass transition,[69] which predicts that

$$D \sim (T - T_{MCT})^\gamma \qquad (3)$$

where T_{MCT} is the temperature of an avoided vitrification of the ideal MCT. Although discussion continues concerning the region of validity of the MCT approach, the phenomenological appearance of power-law behavior immediately below T_A is widely acknowledged. Moreover, power-law behavior of D in water at atmospheric pressure has been appreciated since the 1970s.[70] This power-law behavior of D in water was first interpreted as possible evidence for an underlying spinodal singularity, but more recently it has been connected with the MCT approach.[71−74] Accordingly, we fit separately the isobaric and isochoric data for D to eq 3 to evaluate the locus of T_{MCT} in the phase diagram, which we discuss below. Fits must be considered along both isochoric and isobaric paths, because
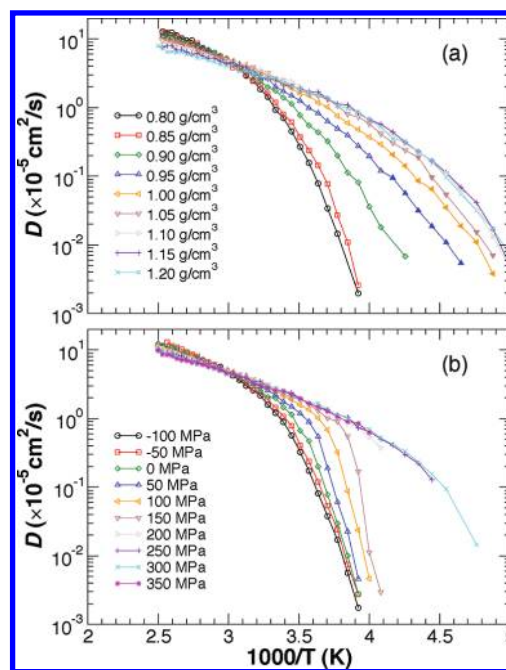

Figure 3. Diffusion coefficient D as a function of T along (a) isochores and (b) isobars. Along isochores the solid symbols indicate systems from the unstable zone of the coexistence region. No data for unstable states are shown along the isobars in (b), because D is a multivalued function of pressure in this region (Figure 2c,d). We show only a selection of densities and pressures to avoid overcrowding the figure.

the diffusivity exponent γ will depend on the path of the approach to T_{MCT}. Additionally, care must be taken in making
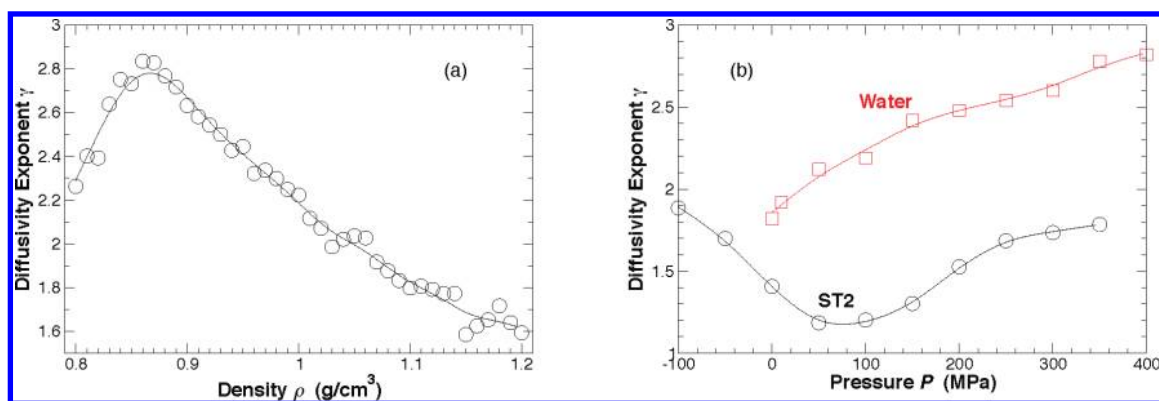
Figure 4. Diffusivity exponent γ as a function of (a) density and (b) pressure. The pressure dependence of γ parallels that of water in the region where experimental data are available. Experimental data are from ref 65 and 66. The lines are only a guide to the eye.

this fit, because it is apparent from Figure 3 that it appears D may return to Arrhenius behavior at lower T, a phenomenon we will discuss in detail in the following section. Therefore, we have excluded data where the behavior may revert to Arrhenius.

We find that the diffusivity exponent γ is nonmonotonic with density, reaching a maximum of ≈ 2.8 at $\rho \approx 0.88$ g/cm^3 (Figure 4). The exponent γ is also nonmonotonic as a function of pressure. A comparison with experimental data for γ shows that the behavior of γ for ST2 is roughly parallel in the region where both experimental and simulation data are available. This is in contrast with the SPC/E model of water, where the opposite pressure dependence occurs.[74]

To summarize the properties of D, we collect the resulting characteristic features from the isothermal, isochoric, and isobaric plots (Figures 2 and 3) and plot them together with the known thermodynamic features. We show these features, along with a colormap for D, in the $\rho-T$ plane and in the $P-T$ plane in Figure 5. As expected from ref 75, the locus D_{max} lies outside the region of negative entropy−volume correlations, delineated by the locus of extrema of density ρ_{ext}. The existence of a maximum in D also results in nonmonotonic behavior of T_A and T_{MCT}, because these temperatures represent a nearly constant value of D. The locus of T_{MCT} is nearly coincident with the lower bound of our simulated data, because this also represents the time scale where simulations become prohibitively lengthy. We also show the locus $T_\times$ of the breakdown of the Stokes−Einstein (SE) relationship from refs 60 and 76. It is interesting to note that $T_\times > T_{MCT}$, because the breakdown of the SE relation is often linked with T_{MCT}. For low pressure, $T_\times$ is correlated with (but not coincident with) the extrema of the specific heat.[76] Finally, the shape of the loci T_A, T_{MCT}, and T_X are all similar, with the nonmonotonic behavior becoming more pronounced with lower T.

STRUCTURE AND DYNAMICS OF THE LOW DENSITY LIQUID PHASE

One of the most challenging aspects of the liquid−liquid phase transition in ST2 water is characterizing the properties of the LDL phase. As shown in the previous section, at low density ($\rho < \rho_c$ or $P < P_c$) the value of D decreases far more rapidly as T decreases than for $\rho > \rho_c$. Obtaining equilibrium values for both structural and dynamical properties of the LDL phase is therefore particularly demanding of computational resources. In this section, we examine the behavior of the liquid in this low density

regime and show that many properties of the LDL phase can be determined from the behavior observed in the region accessible to our simulations.

In particular, we focus on states along the optimal density $\rho = 0.83$ g/cm^3 isochore. As shown in Figure 1b, this density approximately corresponds to a minimum in isotherms of U versus V, indicating that the structure of the random tetrahedral network (RTN) is particularly well developed at this density. We therefore expect that the characteristic properties of the LDL phase will be most prominent at this density.

To complement the $N = 1728$ simulation results described in the previous section, we examine an ensemble of 40 independently initialize and equilibrate simulations along the $\rho = 0.83$ g/cm^3 isochore for a system of size $N = 216$. The smaller system size allows us to probe longer time scales than for $N = 1728$. In addition, by averaging our results at each T over the 40 independent runs, we can significantly reduce the statistical error of our results. We thus use these smaller systems to carefully parse the behavior of the low-density liquid.

To evaluate the dynamical behavior of the $N = 216$ system at $\rho = 0.83$ g/cm^3, in each of the 40 runs, the diffusion coefficient is estimated from $D = \langle r^2 \rangle / 6t$, where $\langle r^2 \rangle$ is the mean squared displacement at the end of the run, and t is the time of the run. All our production runs for $N = 216$ are carried out until $\langle r^2 \rangle = 1.0$ nm^2, or $t = 0.5$ ns, whichever takes longer to achieve. At the lowest T (255 K), the longest runs require up to 350 ns. We then average the results over the 40 runs.

The results for D as a function of T are shown in an Arrhenius plot in Figure 6. Consistent with the results of Figure 3, we find that the T-dependence of D crosses over from non-Arrhenius (fragile) at higher T to Arrhenius at the lowest T with an activation energy $E = 114$ kJ/mol. This appears to be the beginning of a "fragile-to-strong crossover" (FSC); such behavior has been observed and studied in a number of systems in which the RTN-like structure emerges at low T.[25,62,63,73,77−79] Because we have not yet reached the low energy RTN, the activation energy has not reached its low-T asymptotic value. The approach to the RTN can exhibit intermediate Arrhenius behavior over several decades in D before reaching the asymptotic limit.[25]

To support our interpretation that we are approaching strong liquid behavior as T decreases, we test the expectation that the FSC is associated with the approach to the lowest lying minima of the liquid's potential energy landscape (PEL). To confirm this behavior in ST2 water, we carry out conjugate gradient quenches
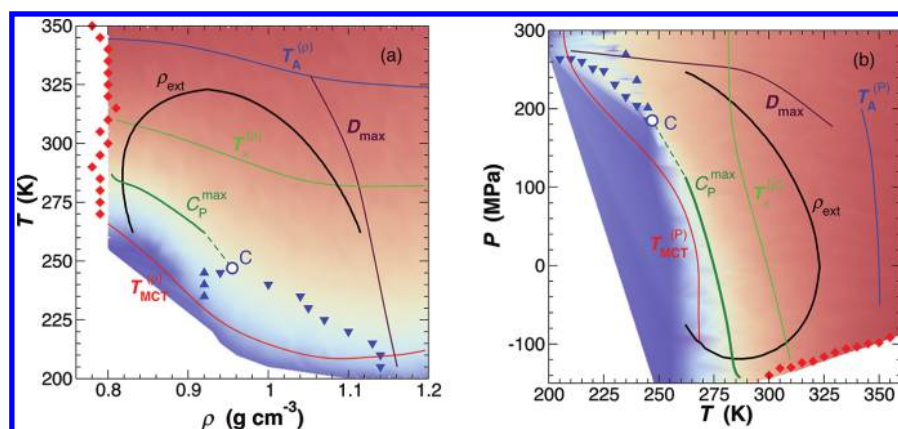
Figure 5. (a) $T-\rho$ and (b) $P-T$ phase diagrams, combined with the dynamical features determined here: D_{max}, the locus of extrema of D along isotherms; $T_A^{(X)}$, the onset of non-Arrhenius behavior; $T_{\times}^X$, the breakdown of Stokes–Einstein behavior (from refs 60 and 76); T_{MCT}^X, the extrapolated mode-coupling divergence temperature. The superscript X for the last three loci indicates whether the locus was determined along isochores ($X = \rho$) or isobars ($X = P$). The color map indicates the value of $\log D$; red (blue) represents the highest (lowest) values of D. The liquid–gas spinodal is indicated by red diamonds; the liquid–liquid spinodals are indicated by blue triangles. The liquid–liquid critical point location is indicated by the open circle. The locus of specific heat maxima C_P^{max} tracks the maxima of C_P along isobars; the dotted portion of the line is an extrapolation to the critical point, where C_P diverges. ρ_{ext} labels the locus of density extrema; inside the ρ_{ext} locus, the isobaric expansivity is negative, and outside it is positive. All thermodynamic data are from ref 53.
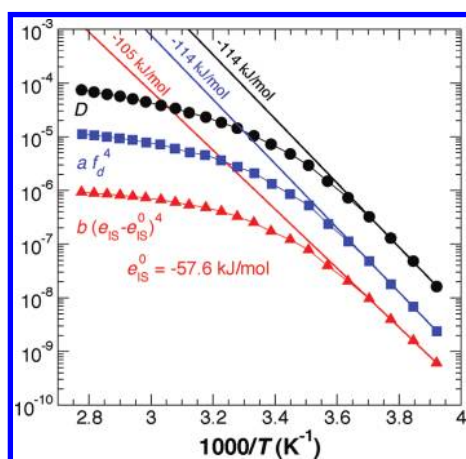

Figure 6. Arrhenius plots of D, $a \cdot f_d^4$, and $b \cdot (e_{IS} - e_{IS}^0)^4$. f_d is the fraction of defects found in instantaneous liquid configurations. All curves are for liquid ST2 water along the $\rho = 0.83$ g/cm^3 isochore, as determined from our $N = 216$ simulations. D is plotted in cm^2/s, and f_d^4 and $(e_{IS} - e_{IS}^0)$ are multiplied by arbitrary constants a and b to facilitate comparison within the same plot. The straight lines are fits to an expression proportional to $\exp(-E_a/RT)$ for the four lowest T points along each curve; each of these lines is labeled by the activation energy E_a obtained from the fit.

Figure 7. Behavior of liquid ST2 water as a function of T along the $\rho = 0.83$ g/cm^3 isochore, determined from the $N = 216$ simulations. (a) $U - 3RT$ for the liquid (circles), and for crystalline ice I$_h$ (solid line), compared with the behavior of e_{IS} (squares) from the inherent structures. The dotted green line shows the estimated limiting e_{IS}^0 for amorphous states, larger than the ice energy. (b) Isochoric heat capacity C_V of the liquid. The solid line is only a guide for the eye. (c) Fraction of defects f_d as found from instantaneous (circles) and inherent structure (squares) configurations of the liquid.

of a large number of configurations (at least 400 for each value of T studied) to evaluate the average energy of a liquid configuration when quenched to its nearest local minimum of the PEL, referred to as the average inherent structure energy, e_{IS}.

In Figure 7a we show both U and e_{IS} as a function of T for $\rho = 0.83$ g/cm^3. In both cases we find that an inflection occurs in the vicinity of $T = 285$ K and that at lower T the rate of decrease of the energy slows with decreasing T. Figure 7a also shows U for the ice I$_h$ crystal, the value of which sets a lower bound on e_{IS} for the liquid. The relative shape and position of these curves suggests that the energy of the low density liquid is approaching
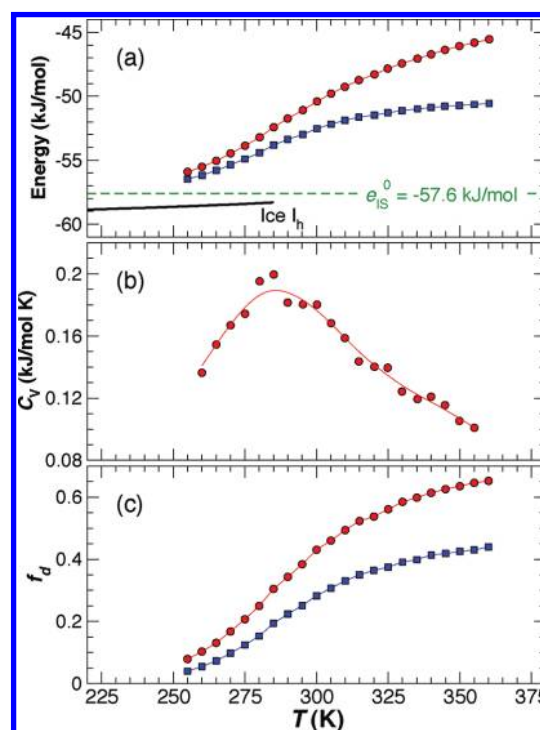
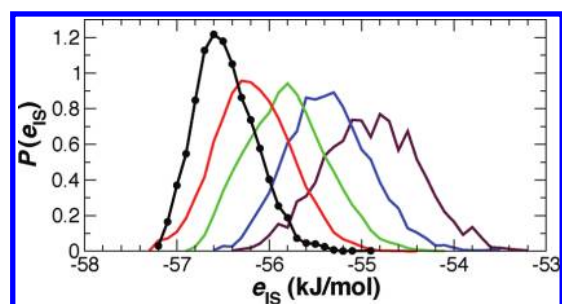a low T limit associated with the "bottom" of the liquid PEL that lies above the crystal state.

Figure 8. Probability distributions of e_{IS} for the liquid from the $N = 216$ simulations, along the $\rho = 0.83$ g/cm^3 isochore. From left to right, $T = 255-275$ K, in 5 K steps.

The approach of the liquid to the bottom of the PEL is also confirmed in Figure 8, which plots the sampled probability distribution of the set of e_{IS} values obtained at low T. Although at high T the distributions are approximately Gaussian, at the lowest $T = 255$ K the distribution has become distinctly skewed and narrower, reflecting the approach to a finite lower bound for the possible values of e_{IS}. We assume that the approach of e_{IS} toward its minimum value e_{IS}^0 obeys

$$e_{IS} = e_{IS}^0 + Be^{-A_{IS}/RT} \qquad (4)$$

and estimate e_{IS}^0 by fitting e_{IS} to this form over the range of T in which D appears to follow an Arrhenius behavior. We approximate this range as the lowest four T shown in Figure 6 and obtain $e_{IS}^0 = -57.6$ kJ/mol. As expected for a liquid, this value is above that of the value of U for the crystal, ice I$_h$. The limiting strong behavior will only be apparent when the system nears e_{IS}^0. We notice that the value of e_{IS}^0 is almost exactly half of the value of the activation energy for diffusion.

This can be understood by considering a picture where diffusion is dominated by single particle displacements that require the breaking of bonds with the four nearest neighbors. Because each bond connects two molecules, we can evaluate the binding energy per bond $E_b \approx e_{IS}^0/2 = -28.8$ kJ/mol, which is larger than the bare HB energy $E_{HB} \approx 20$ kJ/mol,[56,57] because E_b includes nonbonded interactions. Hence the activation energy for diffusion is roughly four times the binding energy, supporting the view that D at these conditions is related to single particle motion, rather than collective displacements.

We also note in Figure 7b that a maximum in the isochoric heat capacity C_V occurs in the vicinity of $T = 285$ K, and as expected, coincides with the inflections of U and e_{IS} shown in Figure 7a. This thermodynamic signature emphasizes that even though all our data at $\rho = 0.83$ g/cm^3 lie above T_c, for $T < 285$ K we have crossed into the regime in which the properties of the liquid are increasingly dominated by the LDL phase, which is distinct from the HDL phase for $T < T_c$.

To provide some structural insight into the dynamical behavior along the $\rho = 0.83$ g/cm^3 isochore, we examine the role of defects in the RTN structure of the liquid. In a perfect RTN, all molecules would have exactly four nearest neighbors (nn's) within a distance given by the first minimum of the oxygen−oxygen radial distribution function. This distance is approximately 0.35 nm in ST2 water at $\rho = 0.83$ g/cm^3.[57] We thus define the fraction of RTN defects f_d as the average fraction of molecules in the system that do *not* have four nn's within a distance of 0.35 nm; hence such defect molecules will have either more than or less than four nn's. f_d is plotted as a function of T in Figure 7c, as
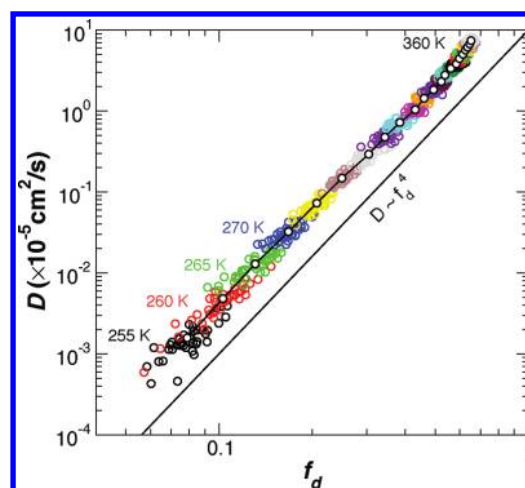

Figure 9. Parametric plot of D versus f_d (squares) for the liquid from the $N = 216$ simulations, along the $\rho = 0.83$ g/cm^3 isochore, from $T = 255$ K (bottom left) to 360 K (top right). In this plot, f_d is evaluated from the instantaneous configurations of the liquid. For each T, we also show the "cloud" of points giving the values of D and f_d obtained from each of the 40 independent simulations conducted at each T. The straight line has a slope of 4.

obtained both from instantaneous liquid configurations and from inherent structures. In both cases we find that f_d decreases as T decreases, passes through an inflection near $T = 285$ K, and approaches zero at our lowest T. Indeed, as shown in Figure 6, we find that the approach of f_d to zero at low T closely follows an exponential decay and, in particular, that the defect activation energy E_a obtained by plotting f_d^4 is approximately equal to the value of E_a obtained by fitting D to an Arrhenius law at low T. Because $E_a \approx 4E_b$, f_d is approximately proportional to the exponential of E_b/RT; hence, f_d essentially measures the probability that a single bond is broken.

To test if the relation between D and f_d holds at higher T (where the behavior is non-Arrhenius), we present in Figure 9 a parametric plot of D versus f_d over the entire T range studied at $\rho = 0.83$ g/cm^3, from $T = 360$ to 255 K. Except for some deviations at the highest T, we find a remarkably consistent behavior in which D varies as a power law in f_d over almost four decades, and with an exponent very close to 4. This result strongly suggests that the liquid at this density can be understood as a disrupted RTN, and that the localized excitations of this RTN (i.e., the defects) control the transport properties of the liquid.

The relation between D and f_d can be anticipated by works on colloids and nanoparticles with highly directional interactions. In particular, it was found that, in systems of patchy colloids with four sticky spots in a tetrahedral geometry[62] and in nanoparticles linked by DNA with tetrahedral orientation,[80,81] D is given by the fourth power of the fraction of broken bonds, $D \sim f^4$. One possible explanation for this behavior is that D is controlled by the diffusion process of the particles that have four broken bonds, and that are thus free to wander around in the available empty space, searching for the rare free dangling ends—i.e., for the rare sites of the network with incomplete bonding—to stick. Indeed, if this is the case, D is proportional in a first approximation to the fraction of unbonded particles, and this fraction scales with f^4. It is important to remember that liquid water at this density belongs[82] to the category of so-called empty liquids,[83] i.e., liquids in which

the fraction of space occupied by a space-filling representation of the molecules is significantly smaller than the close packing value. For the case of liquid water, the corresponding effective packing fraction, when molecules are considered as hard-spheres of diameter 0.28 nm (the mean hydrogen bond length), is 38%.

The comparison between water and these tailored tetrahedral systems[62,80,81] can also help clarify the connection between the activation energy of the dynamics and the bonding energy. Indeed, in these systems, it is clear that the activation energy for diffusion is given by 4 times the bond energy, because the interactions are short-ranged and there is no energy contribution from nonbonded neighbors. For ST2, each hydrogen bond has a strength of $E_{HB} \approx 20$ kJ/mol,[56,57] significantly less (by 9 kJ/mol) than the overall binding energy per bond E_b at the lowest T simulated. If breaking of HBs is the limiting factor in diffusion, we can anticipate that the asymptotic activation energy for diffusion may decrease to a limiting value of ≈ 80 kJ/mol, similar to the low-T value (74 kJ/mol) estimated for water.[25]

■ SUMMARY

In conclusion, we have provided a comprehensive survey of the diffusive properties of the ST2 water model in the vicinity of the liquid−liquid transition. Our results demonstrate that the structural and dynamical properties of the LDL phase that becomes a thermodynamically distinct liquid phase for $T < T_c$ are already well established in the liquid at low density for $T > T_c$. The LDL phase is here revealed as a highly structured liquid, whose properties are dominated by the progressive emergence of a RTN structure as T decreases. In this sense, the properties of the LDL phase are entirely consistent with those of low density amorphous ice, as determined in experiments. Finally, we show that the dynamics of the LDL appears to be fully controlled by the presence of defects of the network, whose concentration is controlled by the bond energy.

■ AUTHOR INFORMATION

Corresponding Author
*E-mail: P.H.P., ppoole@stfx.ca; F.S., francesco.sciortino@uniroma1.it; F.W.S., fstarr@wesleyan.edu.

Present Addresses
§Department of Applied & Computational Math, California Institute of Technology, Pasadena, CA 91125.

■ ACKNOWLEDGMENT

■ REFERENCES

(1) Eisenberg, D.; Kauzmann, W. *The Structure and Properties of Water*; Oxford University Press: New York, 1969.

(2) Franks, F., Ed. *Water: A Comprehensive Treatise*; Plenum Press: New York, 1972; Vols. 1−7.

(3) Stanley, H. E.; Teixeira, J. *J. Chem. Phys.* **1980**, *73*, 3404–3422.

(4) Geiger, A.; Stanley, H. E. *Phys. Rev. Lett.* **1982**, *49*, 1749–1752.

(5) Blumberg, R. L.; Stanley, H. E.; Geiger, A.; Mausbach, P. *J. Chem. Phys.* **1984**, *80*, 5230–5241.

(6) Sciortino, F.; Poole, P.; Stanley, H. E.; Havlin, S. *Phys. Rev. Lett.* **1990**, *64*, 1686–1689.

(7) Starr, F. W.; Nielsen, J. K.; Stanley, H. E. *Phys. Rev. Lett.* **1999**, *82*, 2294–2297.

(8) Han, S.; Kumar, P.; Stanley, H. E. *Phys. Rev. E* **2009**, *79*, 041202.

(9) Poole, P. H.; Sciortino, F.; Essmann, U.; Stanley, H. E. *Nature* **1992**, *360*, 324–328.

(10) Sastry, S.; Sciortino, F.; Stanley, H. E. *J. Chem. Phys.* **1993**, *98*, 9863–9872.

(11) Poole, P. H.; Sciortino, F.; Essmann, U.; Stanley, H. E. *Phys. Rev. E* **1993**, *48*, 3799.

(12) Poole, P. H.; Essmann, U.; Sciortino, F.; Stanley, H. E. *Phys. Rev. E* **1993**, *48*, 4605–4610.

(13) Poole, P. H.; Sciortino, F.; Grande, T.; Stanley, H. E.; Angell, C. A. *Phys. Rev. Lett.* **1994**, *73*, 1632–1635.

(14) Sastry, S.; Debenedetti, P.; Sciortino, F.; Stanley, H. E. *Phys. Rev. E* **1996**, *53*, 6144–6154.

(15) Harrington, S. T.; Zhang, R.; Poole, P. H.; Sciortino, F.; Stanley, H. E. *Phys. Rev. Lett.* **1997**, *78*, 2409–2412.

(16) Sciortino, F.; Poole, P. H.; Essmann, U.; Stanley, H. E. *Phys. Rev. E* **1997**, *55*, 727.

(17) Sadr-Lahijany, M. R.; Scala, A.; Buldyrev, S. V.; Stanley, H. E. *Phys. Rev. Lett.* **1998**, *81*, 4895–4898.

(18) Mishima, O.; Stanley, H. E. *Nature* **1998**, *392*, 192.

(19) Starr, F. W.; Bellissent-Funel, M.-C.; Stanley, H. E. *Phys. Rev. E* **1999**, *60*, 1084–1087.

(20) Meyer, M.; Stanley, H. E. *J. Phys. Chem. B* **1999**, *103*, 9728–9730.

(21) Scala, A.; Starr, F. W.; Nave, E. L.; Stanley, H. E.; Sciortino, F. *Phys. Rev. E* **2000**, *62*, 8016–8020.

(22) Franzese, G.; Malescio, G.; Skibinsky, A.; Buldyrev, S. V.; Stanley, H. E. *Nature* **2001**, *409*, 692–695.

(23) Giovambattista, N.; Starr, F. W.; Sciortino, F.; Buldyrev, S. V.; Stanley, H. E. *Phys. Rev. E* **2002**, *65*, 041502.

(24) Yamada, M.; Mossa, S.; Stanley, H. E.; Sciortino, F. *Phys. Rev. Lett.* **2002**, *88*, 195701.

(25) Starr, F. W.; Angell, C. A.; Stanley, H. E. *Physica A* **2003**, *323*, 51–66.

(26) Buldyrev, S. V.; Stanley, H. E. *Physica A* **2003**, *330*, 124–129.

(27) Giovambattista, N.; Stanley, H. E.; Sciortino, F. *Phys. Rev. Lett.* **2003**, *91*, 115504.

(28) Skibinsky, A.; Buldyrev, S. V.; Franzese, G.; Malescio, G.; Stanley, H. E. *Phys. Rev. E* **2004**, *69*, 061206.

(29) Giovambattista, N.; Stanley, H. E.; Sciortino, F. *Phys. Rev. Lett.* **2005**, *94*, 107803.

(30) Xu, L.; Kumar, P.; Buldyrev, S. V.; Chen, S.-H.; Poole, P. H.; Sciortino, F.; Stanley, H. E. *Proc. Natl. Acad. Sci. U. S. A.* **2005**, *102*, 16558–16562.

(31) Giovambattista, N.; Stanley, H. E.; Sciortino, F. *Phys. Rev. E* **2005**, *72*, 031510.

(32) Kumar, P.; Buldyrev, S. V.; Starr, F.; Giovambattista, N.; Stanley, H. E. *Phys. Rev. E* **2005**, *72*, 051503.

(33) Kumar, P.; Yan, Z.; Xu, L.; Mazza, M. G.; Buldyrev, S. V.; Sastry, S.-H. C. S.; Stanley, H. E. *Phys. Rev. Lett.* **2006**, *97*, 177802.

(34) Kumar, P.; Buldyrev, S. V.; Becker, S. L.; Poole, P. H.; Starr, F. W.; Stanley, H. E. *Proc. Natl. Acad. Sci. U. S. A.* **2007**, *104*[23], 9575–9579.

(35) Yan, Z.; Buldyrev, S. V.; Kumar, P.; Giovambattista, N.; Stanley, H. E. *Phys. Rev. E* **2008**, *77*, 042201.

(36) Xu, L.; Buldyrev, S. V.; Giovambattista, N.; Angell, C. A.; Stanley, H. E. *J. Chem. Phys.* **2009**, *130*, 054505.

(37) Xu, L.; Mallamace, F.; Yan, Z.; Starr, F. W.; Buldyrev, S. V.; Stanley, H. E. *Nat. Physics* **2009**, *5*, 565–569.

(38) Stokely, K.; Mazza, M. G.; Stanley, H. E.; Franzese, G. *Proc. Natl. Acad. Sci. U. S. A.* **2010**, *107*, 1301–1306.

(39) Mishima, O.; Stanley, H. E. *Nature* **1998**, *396*, 329.

(40) Debenedetti, P. G.; Stanley, H. E. *Phys. Today* **2003**, *56*, 40–46.

(41) Mishima, O.; Calvert, L. D.; Whalley, E. *Nature* **1985**, *314*, 76.

(42) Mishima, O. *J. Chem. Phys.* **1994**, *100*, 5910–5912.

(43) Angell, C. A. *Annu. Rev. Phys. Chem.* **2004**, *55*, 559–583.

(44) Loerting, T.; Giovambattista, N. *J. Phys.: Condens. Matter* **2006**, *18*, R919–R977.

(45) Sastry, S.; Angell, C. A. *Nat. Mater.* **2003**, *2*, 739–43.

(46) Poole, P. H.; Hemmati, M.; Angell, C. A. *Phys. Rev. Lett.* **1997**, *79*, 2281–2284.

(47) Hemmati, M.; Moynihan, C.; Angell, C. *J. Chem. Phys.* **2001**, *115*, 6663–6671.

(48) Hsu, C. W.; Largo, J.; Sciortino, F.; Starr, F. W. *Proc. Natl. Acad. Sci. U. S. A.* **2008**, *105*, 13711–13715.

(49) Dai, W.; Hsu, C. W.; Sciortino, F.; Starr, F. W. *Langmuir* **2010**, *26*, 3601–3608.

(50) Kumar, P.; Buldyrev, S.; Sciortino, F.; Zaccarelli, E.; Stanley, H. *Phys. Rev. E* **2005**, *72*, 021501.

(51) Stillinger, F. H.; Rahman, A. *J. Chem. Phys.* **1974**, *60*, 1545.

(52) Paschek, D.; Geiger, A. *J. Phys. Chem. B* **1999**, *103*, 4139.

(53) Poole, P. H.; Saika-Voivod, I.; Sciortino, F. *J. Phys.: Condens. Matter* **2005**, *17*, L431–L437.

(54) Liu, Y.; Panagiotopoulos, A. Z.; Debenedetti, P. G. *J. Chem. Phys.* **2009**, *131*, 104508.

(55) Cuthbertson, M.; Poole, P. H. *Phys. Rev. Lett.* **2011**, *106*, 115706.

(56) Sciortino, F.; Fornili, S. L. *J. Chem. Phys.* **1989**, *90*, 2786–2792.

(57) Sciortino, F.; Geiger, A.; Stanley, H. E. *J. Chem. Phys.* **1992**, *96*, 3857.

(58) Sciortino, F.; Geiger, A.; Stanley, H. E. *Phys. Rev. Lett.* **1990**, *65*, 3452–3455.

(59) Sciortino, F.; Geiger, A.; Stanley, H. E. *Nature* **1991**, *354*, 218–221.

(60) Becker, S. R.; Poole, P. H.; Starr, F. W. *Phys. Rev. Lett.* **2006**, *97*, 055901.

(61) Allen, M. P.; Tildesley, D. J. *Computer Simulation of Liquids*; Oxford University Press: Oxford, U.K., 1987.

(62) DeMichele, C.; Gabrielli, S.; Tartaglia, P.; Sciortino, F. *J. Phys. Chem. B* **2006**, *110*, 8064–8079.

(63) De Michele, C.; Tartaglia, P.; Sciortino, F. *J. Chem. Phys.* **2006**, *125*, 204710.

(64) Zaccarelli, E.; Sciortino, F.; Tartaglia, P. *J. Chem. Phys.* **2007**, *127*, 174501.

(65) Prielmeier, F. X.; Lang, E. W.; Speedy, R. J.; Lüdemann, H.-D. *Phys. Rev. Lett.* **1987**, *59*, 1128–1131.

(66) Prielmeier, F. X.; Lang, E. W.; Speedy, R. J.; Lüdemann, H.-D. *Ber. Bunsen-Ges. Phys. Chem.* **1988**, *92*, 1111.

(67) Harrington, S.; Poole, P. H.; Sciortino, F.; Stanley, H. E. *J. Chem. Phys.* **1997**, *107*, 7443–7450.

(68) Sastry, S.; Debenedetti, P. G.; Stillinger, F. H. *Nature* **1998**, *393*, 554.

(69) Götze, W. In *Les Houches Summer Schools of Theoretical Physics Session LI (1989)*; Hansen, J. P., Levesque, D., Zinn-Justin, J., Eds.; North-Holland: Amsterdam, 1991; pp 287—503.

(70) Angell, C. A. In *Water: A Comprehensive Treatise*; Franks, F., Ed.; Plenum: New York, 1982.

(71) Gallo, P.; Sciortino, F.; Tartaglia, P.; Chen, S. H. *Phys. Rev. Lett.* **1996**, *76*, 2730.

(72) Sciortino, F.; Gallo, P.; Tartaglia, P.; Chen, S.-H. *Phys. Rev. E* **1996**, *54*, 6331–6343.

(73) Starr, F. W.; Harrington, S.; Sciortino, F.; Stanley, H. E. *Phys. Rev. Lett.* **1999**, *82*, 3629–3632.

(74) Starr, F. W.; Sciortino, F.; Stanley, H. E. *Phys. Rev. E* **1999**, *60*, 6757–6768.

(75) Errington, J.; Debenedetti, P. G. *Nature* **2001**, *409*, 318–321.

(76) Kumar, P.; Buldyrev, S. V.; Becker, S. R.; Poole, P. H.; Starr, F. W.; Stanley, H. E. *Proc. Natl. Acad. Sci. U. S. A.* **2007**, *104*, 9575–9.

(77) Horbach, J.; Kob, W. *Phys. Rev. B* **1999**, *60*, 3169–3181.

(78) Saika-Voivod, I.; Poole, P. H.; Sciortino, F. *Nature* **2001**, *412*, 514–517.

(79) Xu, L.; Kumar, P.; Buldyrev, S.; Chen, S.; Poole, P. H.; Sciortino, F.; Stanley, H. *Proc. Natl. Acad. Sci. U. S. A.* **2005**, *102*, 16558–16562.

(80) Starr, F. W.; Sciortino, F. *J. Phys.: Condens. Matter* **2006**, *18*, L347–L353.

(81) Largo, J.; Starr, F. W.; Sciortino, F. *Langmuir* **2006**, *23*, 5896–5905.

(82) Sciortino, F. *Eur. Phys. J. B* **2007**, *64*, 505–509.

(83) Bianchi, E.; Largo, J.; Tartaglia, P.; Zaccarelli, E.; Sciortino, F. *Phys. Rev. Lett.* **2006**, *97*, 168301–168304.